

Key Points:

- The Schelkunoff kernel for cylindrical media involves higher order modified Bessel functions with higher order azimuthal modal summation
- The Sommerfeld integral converges faster than Schelkunoff integral for large radial separation between source and field points
- The Schelkunoff integral converges faster compared to Sommerfeld integral for large axial separation between source and field points

Correspondence to:



T. Shaikh,
tazeenshaikh@iitkgp.ac.in

Citation:

Shaikh, T., Ghosh, B., Bhattacharya, D., & Sarabandi, K. (2022). Schelkunoff formulation of the Sommerfeld integral for the Hertzian dipole located in the vicinity of cylindrical structures. *Radio Science*, 57, e2022RS007451. <https://doi.org/10.1029/2022RS007451>

Received 15 FEB 2022
Accepted 12 AUG 2022

Schelkunoff Formulation of the Sommerfeld Integral for the Hertzian Dipole Located in the Vicinity of Cylindrical Structures

Tazeen Shaikh¹ , Bratin Ghosh¹ , Dhruvajyoti Bhattacharya², and Kamal Sarabandi³

¹Department of Electronics and Electrical Communication Engineering, Indian Institute of Technology, Kharagpur, India,
²Department of Electronics and Communication Engineering, Indian Institute of Information Technology, Bhagalpur, India,
³Department of Electrical Engineering and Computer Science, University of Michigan, Ann Arbor, MI, USA

Abstract A numerical integration of the Sommerfeld integral is performed using the Schelkunoff formulation for cylindrical media. The Schelkunoff kernel for cylindrical media involves higher order modified Bessel functions with azimuthal summation over higher order modes. As such, the convergence characteristics of the cylindrical integral kernel are strongly dependent on complex linear combinations of higher order Bessel/Hankel/modified Bessel functions, compared to the case of the planar media where only a single Bessel/modified Bessel function of zeroth order is present. Two cylindrical configurations are analyzed using the new formulation, viz. a conducting cylinder and a dielectric-coated conducting cylinder. The branch-point singularity in the first configuration is removed using the angular transformation for the Sommerfeld/Schelkunoff formulations. A path deformation technique is used for the second configuration to address the problem of poles and branch-point singularities on the real axis of integration. The in-depth analysis of the cylindrical kernels and the integrals with variation in the location of the observation point clearly bring out the relative merits of both formulations for the cylindrical configurations, with the TE/TM coupling for the coated cylinder considered.

1. Introduction

Computation of electromagnetic fields radiated by a source in the vicinity of cylindrical structures is often needed in a wide range of applications. The generalized treatment of a point source radiating in a multilayer cylindrical structure was developed by Chew (1995). Electromagnetic radiation in the vicinity of the conducting cylinder was determined (Carter, 1943; Wait, 1959). The method of steepest descent was used to evaluate the far fields for sources in the vicinity of an infinitely long conducting cylindrical antenna (Lucke, 1951; Papas, 1949).

The closed form Green's function of a cylindrically stratified media was formulated (Tokgoz & Dural, 2000) by deforming the integration path from the real axis to the complex domain followed by the general pencil of function (GPOF) technique (Hua & Sarkar, 1989). The closed form Green's function using the rational function fitting method was reported by Okhmatovski and Cangellaris (2004). The spectral domain mixed-potential Green's function was used (Bertuch et al., 2012) for the analysis of a perfect electric conducting (PEC) cylinder coated with a dielectric layer. An asymptotic extraction approach for the spectral domain mixed potential Green's function was developed (Ye et al., 2013) by expressing the reflection and transmission matrices in the ratio form. The evaluation of input impedance and mutual coupling of microstrip antennas on multilayer cylindrical structures were investigated (Karan & Ertürk, 2014). An efficient Green's function technique was proposed (Bhattacharya et al., 2017) for the evaluation of the input impedance of antennas in cylindrical multilayer configurations by decomposition of the spectral Green's function into particular and homogeneous parts. Guidance conditions and radiation characteristics of antennas in multilayer cylindrical configurations were investigated (Bhattacharya et al., 2020).

Numerical integrations on cylindrical Green's functions involve complex integration techniques in order to deal with the convergence of the Sommerfeld integral tail (Ebihara & Chew, 2003; Moon et al., 2014; Xing et al., 2018). Nine range conditioned approximations were used depending on the argument of the cylindrical Bessel/Hankel functions in order to perform the spectral domain integration (Moon et al., 2014). Rescaled representations of modified cylindrical Bessel functions were employed (Xing et al., 2018) to achieve a robust formulation and address the numerical overflow and underflow problems under double-precision arithmetic for

the computation of electric potential due to arbitrary located point electrodes in cylindrically anisotropic layered media. A vertical tail approach was adapted (Ebihara & Chew, 2003) to address the highly oscillating horizontal tail of the Sommerfeld integral in the modeling of a vertical dipole antenna array in a borehole radar.

For the planar problem of a dipole radiating over a half-space, the radiated fields by the dipole are usually expressed by the Sommerfeld integral with transverse spectral expansion of fields. Alternative field solutions for a dipole radiating over a lossy conductor including the axial-transmission, radial-transmission and nonspectral are developed and compared (Michalski & Mosig, 2015b). An extension to the dipole radiation over a multilayer and plasmonic media was reported by Michalski and Mosig (2015a). An alternative expression for fields produced by a dipole above a two-layered structure using longitudinal spectral expansion is presented (Bhattacharyya, 2018a, 2018b) in which it was shown that auxiliary fields need to be added to obtain source free spectral components.

An equivalent expression to the Sommerfeld integral, called the modified Sommerfeld integral was proposed by Schelkunoff (1936). The formulation (Schelkunoff, 1936) used the modified Bessel function of the second kind instead of the Bessel function which was conventionally used. Based on this, a spectral integration along the vertical wavenumber, referred to as the Schelkunoff integral, was used instead of the transverse spectral expansion for the Sommerfeld half space problem (Dyab, Abdallah, et al., 2013; Dyab, Sarkar, et al., 2013; Sarkar et al., 2014). The formulation was used to compute the radiation from a vertical dipole over an imperfect ground (Dyab, Abdallah, et al., 2013; Dyab, Sarkar, et al., 2013). Absolute values of the Sommerfeld and Schelkunoff integrands were compared for various radial and vertical distances, and their relative convergence characteristics with large/small radial/vertical distances from the source were evaluated. It is illustrated that the Schelkunoff integral produces accurate results compared to the Sommerfeld integral for field computation at large radial distances from the source for the vertical electric dipole, by comparing calculated results with experimental data in the literature (Sarkar et al., 2014). The Schelkunoff formulation for the horizontal dipole over an imperfect ground was reported (Dyab et al., 2016), where the faster convergence of the Schelkunoff integral compared to the Sommerfeld was observed for large radial distances from the source.

In the proposed work, a formulation for antenna configurations for the dipole radiating in the vicinity of cylindrical structures is developed. The scattered fields are expressed in terms of modified Bessel functions of the first and the second kind of higher orders instead of Bessel and Hankel functions which are conventionally used in Sommerfeld integral. The presence of higher order azimuthal modes and azimuthal summation over higher order harmonics of Bessel/Hankel/modified Bessel functions in the Sommerfeld and Schelkunoff formulations in the current case is distinctly different from the planar media where only a single Bessel/modified Bessel function of zeroth order is present. Consequently, convergence characteristics in the current case are dominated by complex linear combinations of higher order Bessel/Hankel/modified Bessel functions instead of the Bessel/modified Bessel function of zeroth order only in planar media. The technique is used for the analysis of two cylindrical structures, viz. a conducting cylinder and a dielectric-coated conducting cylinder illustrating two distinct approaches for the evaluation of the Sommerfeld/Schelkunoff integrals. The branch-point singularity in the integration along the real axis is removed by angular spectral representation in the case of the conducting cylinder for the Sommerfeld and Schelkunoff kernels. The parametric path deformation technique is used for the coated conducting cylinder to circumvent the pole and branch-point singularities along the real axis. The results obtained by both the formulations are compared in terms of their integrands as well as integrals for a wide range of field points to illustrate their relative merits for the cylindrical configurations, considering the TE/TM mode coupling for the coated cylinder. Though only a single layer of dielectric coating is considered in the work, the treatment can be extended to a multilayer cylindrical configuration.

The paper is organized as follows. In Section 2, the Sommerfeld formulation is used as a starting point for formulating the Schelkunoff integral. Techniques employed to solve the integrals for the conducting cylinder and for the dielectric-coated conducting cylinder are discussed. In Section 3, a detailed comparison between both the formulations is provided and the results for both the kernels and integrals for the conducting cylinder and the dielectric-coated cylinder are compared. The decay rates of the cylindrical kernels with increasing wavenumber are investigated. The rate of convergence for different field locations is also plotted and compared for both the integrals. Computation time required to achieve the same accuracy in the evaluation of the integrals are compared. The analysis distinctly highlights the relative merits of the two formulations for cylindrical structures. Section 4 contains the conclusion.

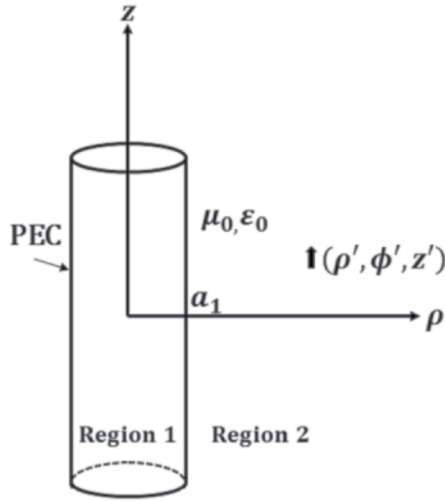


Figure 1. Configuration of a perfectly conducting cylinder excited by a \hat{z} —directed Hertzian dipole.

2. Formulation

2.1. PEC Cylinder

A perfectly conducting cylinder with radius a_1 and excited by a \hat{z} —directed Hertzian dipole located in free space is shown in Figure 1. The locations of the source and field points in the outermost media (free space) are denoted by (ρ', ϕ', z') and (ρ, ϕ, z) respectively. A time variation of $e^{j\omega t}$ is assumed and suppressed throughout the analysis.

The z -component of the electric and magnetic field radiated by the dipole in the vicinity of the cylinder is expressed through the Sommerfeld's identity as (Chew, 1995):

$$\begin{bmatrix} E_z \\ H_z \end{bmatrix} = \frac{-j}{4\pi\omega\epsilon_0} \sum_{n=-\infty}^{\infty} e^{-jn(\phi-\phi')} \int_{-\infty}^{\infty} dk_z e^{-jk_z(z-z')} \bar{F}_{n1}(\rho, \rho') \cdot \bar{D}_2 \quad (1)$$

where

$$\bar{F}_{n1}(\rho, \rho') = H_n^{(2)}(k_{\rho 0}\rho) \left[J_n(k_{\rho 0}\rho') \bar{I} + H_n^{(2)}(k_{\rho 0}\rho') \cdot \bar{R}_{21}^{sm} \right] \quad (2)$$

with

$$\bar{D}_2 = \frac{-j}{2} \begin{bmatrix} k_{\rho 0}^2 \\ 0 \end{bmatrix} \quad (3)$$

$k_{\rho 0}^2 = k_0^2 - k_z^2$ and $k_0 = \omega\sqrt{\mu_0\epsilon_0}$. In Equation 2, $J_n(x)$ and $H_n^{(2)}(x)$ are the Bessel function of first kind and Hankel function of second kind of order n respectively and \bar{I} denotes the 2×2 identity matrix.

$$\bar{R}_{21}^{sm} = \begin{bmatrix} -\frac{J_n(k_{\rho 0}a_1)}{H_n^{(2)}(k_{\rho 0}a_1)} & 0 \\ 0 & -\frac{J'_n(k_{\rho 0}a_1)}{H_n^{(2)'}(k_{\rho 0}a_1)} \end{bmatrix} \quad (4)$$

denotes the local reflection matrix obtained from the boundary conditions at the cylinder-free space interface.

Equation 1 can alternatively be represented by employing the transverse spectral expansion instead of the longitudinal component using Equation 1 by Schelkunoff (1936) as:

$$\begin{bmatrix} E_z \\ H_z \end{bmatrix} = \frac{-1}{2\pi\omega\epsilon_0} \frac{2}{\pi} \sum_{n=-\infty}^{\infty} e^{-jn(\phi-\phi')} \int_0^{\infty} dk_{\rho 0} \frac{k_{\rho 0}}{\sqrt{k_0^2 - k_{\rho 0}^2}} \cos(k_z(z-z')) \bar{F}_{n2}(\rho, \rho') \cdot \bar{D}_2 \quad (5)$$

where

$$\bar{F}_{n2}(\rho, \rho') = K_n\left(\rho\sqrt{k_z^2 - k_0^2}\right) I_n\left(\rho'\sqrt{k_z^2 - k_0^2}\right) \bar{I} + K_n\left(\rho\sqrt{k_z^2 - k_0^2}\right) K_n\left(\rho'\sqrt{k_z^2 - k_0^2}\right) \cdot \bar{R}_{21}^{sc} \quad (6)$$

In Equation 6, $I_n(x)$ and $K_n(x)$ are modified Bessel functions of the first and second kinds respectively of order n , with

$$\bar{R}_{21}^{sc} = \begin{bmatrix} -\frac{I_n\left(a_1\sqrt{k_z^2 - k_0^2}\right)}{K_n\left(a_1\sqrt{k_z^2 - k_0^2}\right)} & 0 \\ 0 & -\frac{I'_n\left(a_1\sqrt{k_z^2 - k_0^2}\right)}{K'_n\left(a_1\sqrt{k_z^2 - k_0^2}\right)} \end{bmatrix} \quad (7)$$

Equation 5 can be interpreted as the Schelkunoff integral for the cylindrical configuration that is obtained by modification in the Sommerfeld integral with change in the integration variable from k_z to k_ρ .

In order to remove the branch-point singularity at $k_z = k_0$ in the evaluation of the Sommerfeld integral in Equation 1, the integral in k_z is transformed to the β domain using the substitution:

$$k_z = k_0 \sin(\beta' + j\beta'') \quad (8)$$

As such, on the main part of the contour $0 \leq k_z \leq k_0$:

$$k_z = k_0 \sin \beta' \quad (9)$$

$$k_{\rho 0} = k_0 \cos \beta' \quad (10)$$

while on the tail part of the integral ($k_0 \leq k_z \leq \infty$):

$$k_z = k_0 \sin\left(\frac{\pi}{2} + j\beta''\right) = k_0 \cosh \beta'' \quad (11)$$

$$k_{\rho 0} = -jk_0 \sinh \beta'' \quad (12)$$

Using the above substitutions, Equation 1 can be represented as:

$$E_z = \frac{-j}{4\pi\omega\epsilon_0} \sum_{n=-\infty}^{\infty} e^{-jn(\phi-\phi')} \left\{ \int_0^{\pi/2} d\beta' (k_0 \cos \beta')^3 \cos(k_0 \sin \beta' (z-z')) (-j)F_{n3}(\rho, \rho') + \int_0^{\infty} d\beta'' (k_0 \sinh \beta'') k_{\rho 0}^2 \cos(k_0 \cosh \beta'' (z-z')) (-j)F_{n4}(\rho, \rho') \right\} \quad (13)$$

where

$$F_{n3}(\rho, \rho') = H_n^{(2)}(\rho k_0 \cos \beta') J_n(\rho' k_0 \cos \beta') + H_n^{(2)}(\rho k_0 \cos \beta') H_n^{(2)}(\rho' k_0 \cos \beta') \left(-\frac{J_n(a_1 k_0 \cos \beta')}{H_n^{(2)}(a_1 k_0 \cos \beta')} \right) \quad (14)$$

$$F_{n4}(\rho, \rho') = H_n^{(2)}(-j\rho k_0 \sinh \beta'') J_n(-j\rho' k_0 \sinh \beta'') + H_n^{(2)}(-j\rho k_0 \sinh \beta'') H_n^{(2)}(-j\rho' k_0 \sinh \beta'') \left(-\frac{J_n(-ja_1 k_0 \sinh \beta'')}{H_n^{(2)}(-ja_1 k_0 \sinh \beta'')} \right) \quad (15)$$

The spatial domain fields can also be evaluated using the Schelkunoff integral in Equation 5. In order to circumvent the branch-point singularity in this case, we use the following substitutions in the complex β plane:

For the main part of the contour $0 \leq k_{\rho 0} \leq k_0$:

$$k_{\rho 0} = k_0 \sin \beta' \quad (16)$$

$$k_z = k_0 \cos \beta' \quad (17)$$

For the tail part ($k_0 \leq k_{\rho 0} \leq \infty$):

$$k_{\rho 0} = k_0 \sin\left(\frac{\pi}{2} + j\beta''\right) = k_0 \cosh \beta'' \quad (18)$$

$$k_z = jk_0 \sinh \beta'' \quad (19)$$

Equation 5 can now be written as:

$$E_z = \frac{-j}{4\pi\omega\epsilon_0} \left(\frac{2}{\pi}\right) \sum_{n=-\infty}^{\infty} e^{-jn(\phi-\phi')} \left\{ \int_0^{\pi/2} d\beta' (-1)(k_0 \sin \beta')^3 \cos(k_0 \cos \beta' (z-z')) F_{n5}(\rho, \rho') \right. \\ \left. + \int_0^{\infty} d\beta'' (k_0 \cosh \beta'')^3 (j) e^{-(z-z')k_0 \sinh \beta''} F_{n6}(\rho, \rho') \right\} \quad (20)$$

where

$$F_{n5}(\rho, \rho') = K_n(j\rho k_0 \sin \beta') I_n(j\rho' k_0 \sin \beta') \\ + K_n(j\rho k_0 \sin \beta') K_n(j\rho' k_0 \sin \beta') \left(-\frac{I_n(ja_1 k_0 \sin \beta')}{K_n(ja_1 k_0 \sin \beta')} \right) \quad (21)$$

$$F_{n6}(\rho, \rho') = K_n(j\rho k_0 \cosh \beta'') I_n(j\rho' k_0 \cosh \beta'') \\ + K_n(j\rho k_0 \cosh \beta'') K_n(j\rho' k_0 \cosh \beta'') \left(-\frac{I_n(ja_1 k_0 \cosh \beta'')}{K_n(ja_1 k_0 \cosh \beta'')} \right) \quad (22)$$

2.2. Dielectric-Coated Conducting Cylinder

The next configuration to be investigated is shown in Figure 2. For the structure, a perfectly conducting cylinder, coated with a dielectric layer is illuminated by a \hat{z} -directed Hertzian dipole located in free space. The radii of the inner and outer cylindrical layers are a_1 and a_2 respectively, with ϵ_2 and μ_2 denoting the permittivity and permeability of the dielectric layer respectively.

For the current two-layered configuration, the radial dependence of fields in Equation 1 is given by:

$$\bar{F}_{n7}(\rho, \rho') = H_n^{(2)}(k_{\rho 0} \rho) \left[J_n(k_{\rho 0} \rho') \bar{I} + H_n^{(2)}(k_{\rho 0} \rho') \cdot \bar{R}_{32}^{sm} \right] \quad (23)$$

where

$$\bar{R}_{32}^{sm} = \bar{R}_{32}^{sm} + \bar{T}_{23}^{sm} \cdot \bar{R}_{21}^{sm} \left(\bar{I} - \bar{R}_{23}^{sm} \cdot \bar{R}_{21}^{sm} \right)^{-1} \cdot \bar{T}_{32}^{sm} \quad (24)$$

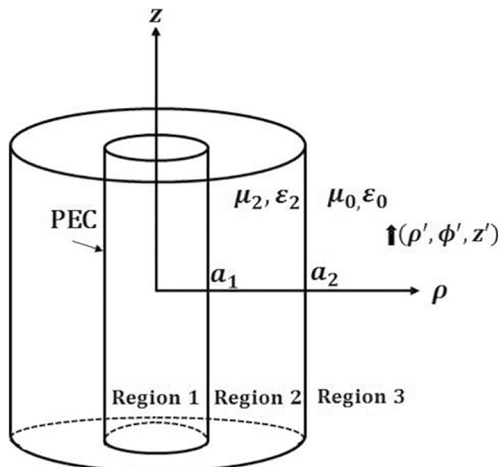


Figure 2. Configuration of a perfectly conducting cylinder coated with a dielectric layer excited by a \hat{z} -directed Hertzian dipole.

The local reflection and transmission matrices in Equation 24 are provided by Chew (1995) with \bar{R}_{21}^{sm} as defined in Equation 4 replaced by the local reflection matrix corresponding to the dielectric—PEC interface. The spatial domain fields for the Sommerfeld case can be obtained by substituting $\bar{F}_{n1}(\rho, \rho')$ by $\bar{F}_{n7}(\rho, \rho')$ in Equation 1.

The radial dependence of fields in the Schelkunoff formulation in Equation 5 is given by:

$$\bar{F}_{n8}(\rho, \rho') = K_n\left(\rho\sqrt{k_z^2 - k_0^2}\right) I_n\left(\rho'\sqrt{k_z^2 - k_0^2}\right) \bar{I} \\ + K_n\left(\rho\sqrt{k_z^2 - k_0^2}\right) K_n\left(\rho'\sqrt{k_z^2 - k_0^2}\right) \cdot \bar{R}_{32}^{sc} \quad (25)$$

where

$$\bar{R}_{32}^{sc} = \bar{R}_{32}^{sc} + \bar{T}_{23}^{sc} \cdot \bar{R}_{21}^{sc} \left(\bar{I} - \bar{R}_{23}^{sc} \cdot \bar{R}_{21}^{sc} \right)^{-1} \cdot \bar{T}_{32}^{sc} \quad (26)$$

In Equation 26,

$$\overline{R}_{32}^{sc} = \overline{D}_{sc}^{-1} \cdot \left[I_n \left(a_2 \sqrt{k_z^2 - k_2^2} \right) \overline{I}_n \left(a_2 \sqrt{k_z^2 - k_0^2} \right) - I_n \left(a_2 \sqrt{k_z^2 - k_0^2} \right) \overline{I}_n \left(a_2 \sqrt{k_z^2 - k_2^2} \right) \right] \quad (27)$$

$$\overline{T}_{23}^{sc} = \overline{D}_{sc}^{-1} \cdot \left[K_n \left(a_2 \sqrt{k_z^2 - k_2^2} \right) \overline{I}_n \left(a_2 \sqrt{k_z^2 - k_2^2} \right) - I_n \left(a_2 \sqrt{k_z^2 - k_2^2} \right) \overline{K}_n \left(a_2 \sqrt{k_z^2 - k_2^2} \right) \right] \quad (28)$$

$$\overline{R}_{23}^{sc} = \overline{D}_{sc}^{-1} \cdot \left[K_n \left(a_2 \sqrt{k_z^2 - k_2^2} \right) \overline{K}_n \left(a_2 \sqrt{k_z^2 - k_0^2} \right) - K_n \left(a_2 \sqrt{k_z^2 - k_0^2} \right) \overline{K}_n \left(a_2 \sqrt{k_z^2 - k_2^2} \right) \right] \quad (29)$$

$$\overline{T}_{32}^{sc} = \overline{D}_{sc}^{-1} \cdot \left[K_n \left(a_2 \sqrt{k_z^2 - k_0^2} \right) \overline{I}_n \left(a_2 \sqrt{k_z^2 - k_0^2} \right) - I_n \left(a_2 \sqrt{k_z^2 - k_0^2} \right) \overline{K}_n \left(a_2 \sqrt{k_z^2 - k_0^2} \right) \right] \quad (30)$$

where

$$\overline{D}_{sc} = \left[\overline{I}_n \left(a_2 \sqrt{k_z^2 - k_2^2} \right) K_n \left(a_2 \sqrt{k_z^2 - k_0^2} \right) - \overline{K}_n \left(a_2 \sqrt{k_z^2 - k_0^2} \right) I_n \left(a_2 \sqrt{k_z^2 - k_2^2} \right) \right] \quad (31)$$

and

$$\overline{C}_n(a_2 x_i) = \frac{1}{a_2 x_i^2} \begin{bmatrix} -j\omega\epsilon_i a_2 x_i C_n'(a_2 x_i) & nk_z C_n(a_2 x_i) \\ nk_z C_n(a_2 x_i) & j\omega\mu_i a_2 x_i C_n'(a_2 x_i) \end{bmatrix} \quad (32)$$

In Equation 32, $x_i = \sqrt{k_z^2 - k_i^2}$ with $i = 0$ or 2 depending on the region of interest. $C_n(x)$ denotes either $I_n(x)$ or $K_n(x)$ corresponding to $\overline{C}_n(x) = \overline{I}_n(x)$ or $\overline{C}_n(x) = \overline{K}_n(x)$ matrices respectively. \overline{R}_{21}^{sc} in Equation 26 is evaluated from Equation 7 with k_0 replaced by k_2 . The spatial domain fields for the Schelkunoff formulation for the coated conducting cylinder can be thereafter obtained by replacing $\overline{F}_{n2}(\rho, \rho')$ in Equation 5 with $\overline{F}_{n8}(\rho, \rho')$.

In addition to the branch-point singularity for the conducting cylinder, the configuration in Figure 2 possesses poles along the original integration path. In order to circumvent this, the path of integration is deformed in the complex k_z -plane for the Sommerfeld case as shown in Figure 3. This path is used instead of the triangular deformation by Karan and Ertürk (2014) to reduce the computational burden of evaluation along two paths above the real axis. The components of the deformed path are defined as follows:

$$\Gamma_1 : k_z = ks_1 \frac{t_1}{T_1}, \quad 0 \leq t_1 \leq T_1 \quad (33)$$

$$\Gamma_2 : k_z = ks_1 + \left((ks_3 - ks_1) \frac{t_2}{\pi} \right) + jT_2 \sin(t_2), \quad 0 \leq t_2 \leq \pi \quad (34)$$

$$\Gamma_3 : k_z = ks_3 + \left((ks_4 - ks_3) \frac{t_3}{T_4 - T_3} \right), \quad 0 \leq t_3 \leq T_4 - T_3 \quad (35)$$

with $ks_1 = T_1 k_0$, $ks_3 = T_3 k_0$, $ks_4 = T_4 k_0$.

In the above, it can be noted that $0.5 \leq T_1 \leq 0.8$. The parameter T_2 controls the deviation of the integration path from the real axis and it should be ensured that the path Γ_2 must meet the real axis after avoiding all pole and branch-point singularities. A value of $T_4 = 13$ ensures convergence for the integrals on Path 3 for all the cases considered in the current work. T_4 would however increase with the increase in the coating permittivity of the dielectric layer, that is constant in this case. The same path deformation is also used for the Schelkunoff integral by replacing k_z with $k_{z\rho}$ in Equations 33–35.

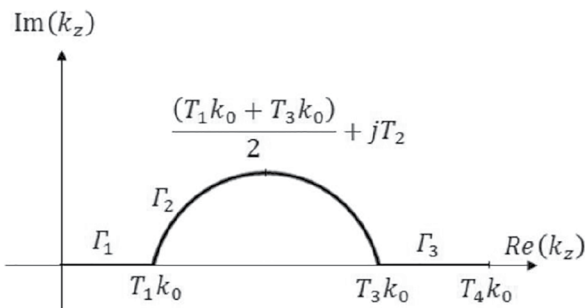


Figure 3. Deformed integration path.

3. Results and Discussion

In this section, the methodology developed in the previous section is used to investigate the convergence characteristics of the Sommerfeld and Schelkunoff kernels for the conducting and the coated conducting cylinders. In addition, the characteristics of the above spectral integrals are also investigated.

The associated cylindrical kernels are distinctly different from that of the planar structures in a number of key points. The presence of azimuthal summation over higher order azimuthal harmonics in cylindrical structures is absent in planar configurations. This has a severe impact on the convergence characteristics since one has to deal with Bessel, Hankel and modified Bessel functions of higher and lower orders both rather than a single zeroth order Bessel or modified Bessel function for planar geometries. Particularly, the local reflection/transmission terms for the cylindrical configuration involve Bessel/Hankel/modified Bessel functions of higher and lower orders compared to the planar media case where the local reflection/transmission coefficients involve spectral wave-numbers only. In addition, though the TE and TM modes are decoupled for planar structures or the conducting cylinder, such is not the case for the dielectric-coated cylinder where the TE/TM modes are coupled. The mode-coupling is incorporated by the reflection and transmission matrix in the formulation instead of the reflection and transmission coefficients for planar structures. Since the reflection/transmission matrices possess complex linear combinations of Bessel/Hankel/modified Bessel functions, this has a considerable impact on the stability and convergence characteristics of the kernel and the spectral integral in both the Sommerfeld and Schelkunoff formulations. In the following, the number of integration points, azimuthal modes, and the integration limits were appropriately chosen to achieve a convergence within 0.1% in the evaluation of the associated kernels and the spectral integrals. The computations are performed using MATLAB version R2019a on a desktop PC with Intel(R) Core(TM) i7-7700 CPU with a 3.6-GHz clock speed.

3.1. PEC Cylinder

In this section, the results for the Sommerfeld and Schelkunoff kernels and evaluation of the spatial domain fields using the Sommerfeld/Schelkunoff formulations for the conducting cylinder are discussed. The comparison of the absolute values of the Sommerfeld and the Schelkunoff kernels for the conducting cylinder is shown in Figure 4, for the cases where the axial separation between the observation and source points is much larger than the radial distance, is equal to the radial distance and is much smaller than the radial distance. The radius of the cylinder is taken as $a_1 = 0.5\lambda_0$ with the Hertzian dipole located at $\rho' = 1\lambda_0$, $z' = 0$, that is maintained constant throughout for all the cases discussed in the following for the conducting cylinder. In order to investigate the convergence behavior of the kernel, the Sommerfeld integral in Equation 1 is folded with the kernel represented as:

$$\tilde{G}_{J_z}^{E_z} = \frac{-j}{4\pi\omega\epsilon_0} \sum_{n=-\infty}^{\infty} e^{-jn(\phi-\phi')} \cos(k_z(z-z')) (-j)k_{\rho 0}^2 H_n^{(2)}(k_{\rho 0}\rho) \left[J_n(k_{\rho 0}\rho') + H_n^{(2)}(k_{\rho 0}\rho') \left(-\frac{J_n(k_{\rho 0}a_1)}{H_n^{(2)}(k_{\rho 0}a_1)} \right) \right] \quad (36)$$

The Schelkunoff kernel can also be explicitly written as:

$$\tilde{G}_{J_z}^{E_z} = \frac{-j}{4\pi\omega\epsilon_0} \frac{2}{\pi} \sum_{n=-\infty}^{\infty} e^{-jn(\phi-\phi')} \frac{-k_{\rho 0}}{\sqrt{k_0^2 - k_{\rho 0}^2}} \cos(k_z(z-z')) K_n\left(\rho\sqrt{k_z^2 - k_0^2}\right) \left[I_n\left(\rho'\sqrt{k_z^2 - k_0^2}\right) + K_n\left(\rho'\sqrt{k_z^2 - k_0^2}\right) \left(-\frac{I_n\left(a_1\sqrt{k_z^2 - k_0^2}\right)}{K_n\left(a_1\sqrt{k_z^2 - k_0^2}\right)} \right) \right] \quad (37)$$

Figure 4a shows the absolute value of the complex kernel in dB plotted against their respective wave numbers k_z/k_0 and $k_{\rho 0}/k_0$ for the Sommerfeld and Schelkunoff formulations at a frequency of 5 GHz for the structure in Figure 1. For the figure, the axial separation between the source and observation points ($10\lambda_0$) is much larger than their radial separation ($1\lambda_0$). A total of 5 eigenmodes are considered for the azimuthal summation in both

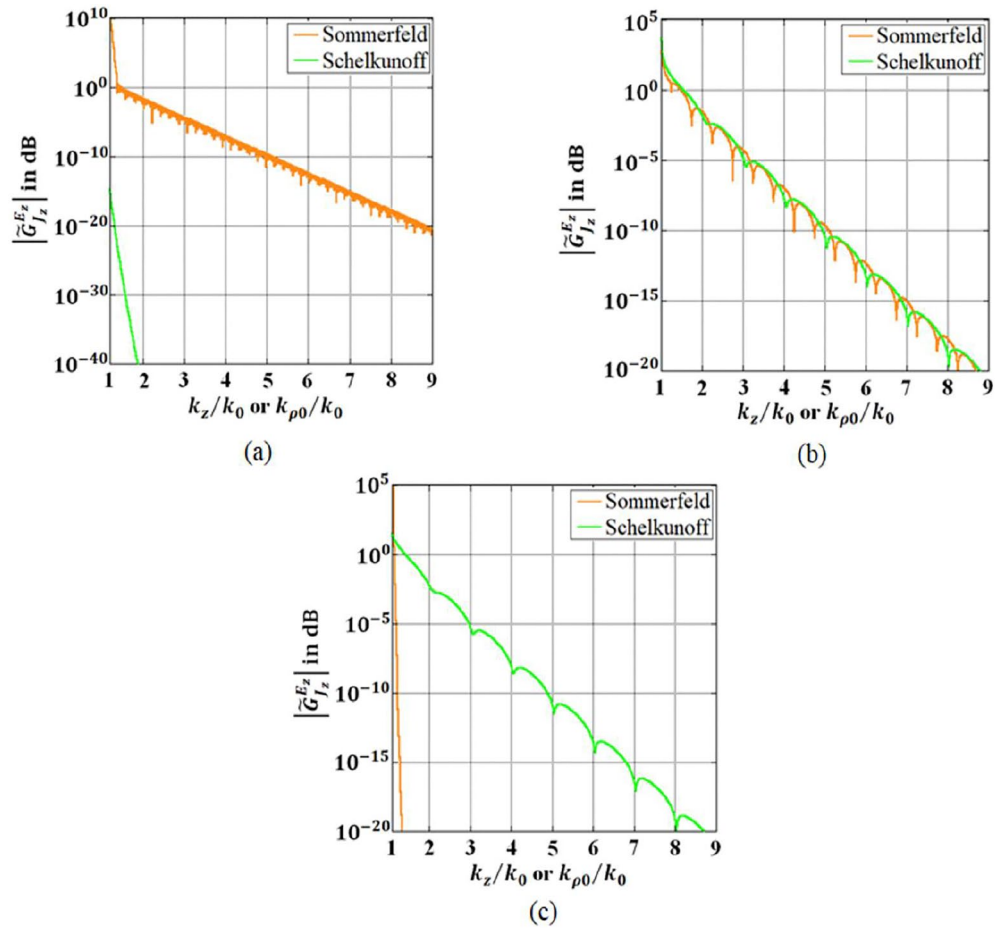


Figure 4. Comparison of the absolute values of the Sommerfeld and the Schelkunoff kernels for the perfectly conducting cylinder with variation in the radial and axial separation between the observation and source points: $a_1 = 0.5\lambda_0$, $\rho' = 1\lambda_0$, and $z' = 0$. (a) $(\rho - \rho') = 1\lambda_0$, $(z - z') = 10\lambda_0$ (b) $(\rho - \rho') = 1\lambda_0$, $(z - z') = 1\lambda_0$, and (c) $(\rho - \rho') = 10\lambda_0$, $(z - z') = 1\lambda_0$.

formulations. It can be observed from Figure 4a that the kernel of Sommerfeld integration is oscillatory and slowly convergent in comparison to the Schelkunoff kernel that exhibits fast convergence with respect to $k_{\rho 0}/k_0$. The faster decay of the Schelkunoff integral can be observed by expressing Equation 5 as:

$$\begin{bmatrix} E_z \\ H_z \end{bmatrix} = \frac{-1}{2\pi\omega\epsilon_0} \frac{2}{\pi} \sum_{n=-\infty}^{\infty} e^{-jn(\phi-\phi')} \left\{ \int_0^{k_0} dk_{\rho 0} \frac{k_{\rho 0}}{\sqrt{k_0^2 - k_{\rho 0}^2}} \cos\left(\sqrt{k_0^2 - k_{\rho 0}^2}(z - z')\right) \bar{F}_{n2}(\rho, \rho') \cdot \bar{D}'_2 \right. \\ \left. + \int_{k_0}^{\infty} dk_{\rho 0} \frac{k_{\rho 0}}{\sqrt{k_0^2 - k_{\rho 0}^2}} e^{-(z-z')\sqrt{k_{\rho 0}^2 - k_0^2}} \bar{F}_{n2}(\rho, \rho') \cdot \bar{D}'_2 \right\} \quad (38)$$

where it can be observed that the integral kernel for $k_{\rho 0} > k_0$ possess an exponential decay that enhances with increasing axial separation between the source and observation points.

The convergence characteristics of the Sommerfeld and the Schelkunoff kernels for the same radial and axial separation between the field and observation points ($1\lambda_0$) is shown in Figure 4b. It is seen that both the kernels have the same convergence rate.

Figure 4c depicts the behavior of the two kernels with the radial separation between the source and observation points ($10\lambda_0$) much greater than their axial separation ($1\lambda_0$). It is observed that the Sommerfeld kernel converges much faster than the Schelkunoff. This can be explained by observing that the term $H_n^{(2)}(k_{\rho 0}\rho)$ on the RHS of $\bar{F}_{n1}(\rho, \rho')$ in Equation 2 leads to the decay in the Sommerfeld kernel for $k_z > k_0$ through the identity $K_n(u) = (\pi/2)(-j)^{n+1}H_n^{(2)}(-ju)$. On the other hand, the term $K_n\left(\rho\sqrt{k_z^2 - k_0^2}\right)$ on the RHS of Equation 6 in the Schelkunoff kernel leads to a slower decay in the kernel due to its conversion to $H_n^{(2)}(k_{\rho 0}\rho)$ over the entire range of integration. It may also be noted that the above results are independent of the absolute location of the dipole. Though not shown, the above conclusions are also valid for the $\hat{\rho}$ - and $\hat{\phi}$ - polarizations of the dipole.

Next, the results of the Sommerfeld and Schelkunoff absolute integral values corresponding to the spatial domain electric field E_z is plotted in Figure 5. Figure 5a shows the variation of electric field with the radial location of the observation point at $z = 100\lambda_0$. It can be observed that the electric fields using the Sommerfeld and Schelkunoff formulations overlap exactly over a large range of radial locations of the observation point upto $\rho = 500\lambda_0$. The spatial domain electric field with variation in the axial location of the observation point is shown in Figure 5b at $\rho = 100\lambda_0$. It is observed that the Sommerfeld and Schelkunoff formulations match over the entire range of z/λ_0 with the onset of oscillations for $z > 300\lambda_0$. It can thus be seen that the Sommerfeld and Schelkunoff formulations agree exactly with each other over a large range of radial and axial distances between the source and observation points. In order to overcome the overflow and underflow problem under finite double-precision arithmetic, range-conditioned cylindrical/modified-cylindrical functions are used in the areas of very large and very small arguments as defined in Moon et al. (2014, 2015).

The convergence characteristics of the Sommerfeld and Schelkunoff absolute integral values corresponding to the spatial domain electric field E_z with the order of the cylindrical functions at $z = 100\lambda_0, \rho = 100\lambda_0$ is shown in Figure 6. It can be observed that convergence in both the Sommerfeld and Schelkunoff formulations is obtained after 9 terms.

Simpson's 1/3 rule have been used for the evaluation of the integrals, with N as the number of samples, as given below:

$$\int_{x_0}^{x_{2n}} f(x)dx \approx \frac{h}{3} [f_0 + 4(f_1 + f_3 + \dots + f_{2n-1}) + 2(f_2 + f_4 + \dots + f_{2n-2}) + f_{2n}] \quad (39)$$

where $h = \frac{x_{2n} - x_0}{N-1} = x_{i+1} - x_i, f(x_i) = f_i$.

In order to compare the efficiency of integral computation for the Sommerfeld and the Schelkunoff formulations, the computation time for evaluating the spatial domain electric fields using the two formulations are now investigated, for yielding the same accuracy. Figure 7a shows the time elapsed for the calculation of the integrals with

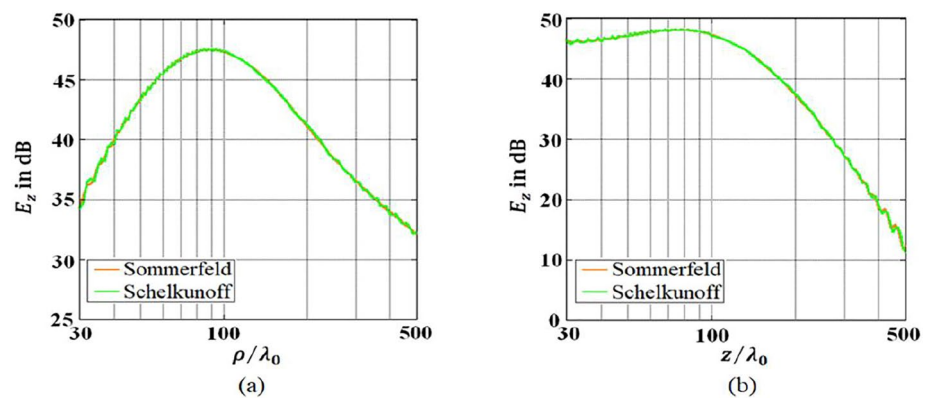


Figure 5. Comparison of the absolute values of the Sommerfeld and the Schelkunoff integrals for the perfectly conducting cylinder at (a) $z = 100\lambda_0$ and (b) $\rho = 100\lambda_0$. All other parameters same as in Figure 4.

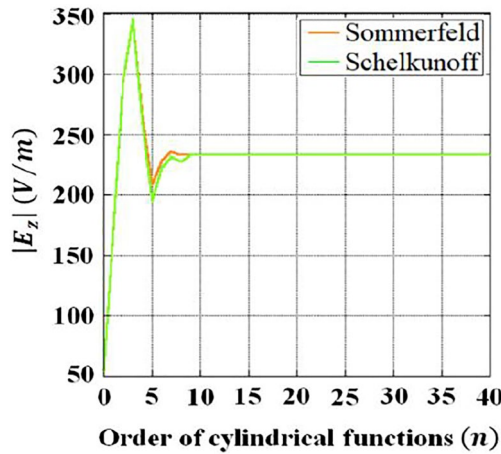


Figure 6. Convergence of the absolute values of the Sommerfeld and the Schelkunoff integrals with order of cylindrical functions for the perfectly conducting cylinder at $z = 100\lambda_0$, $\rho = 100\lambda_0$. All other parameters same as in Figure 4.

respect to variation in radial location of the observation point from $5\lambda_0$ to $500\lambda_0$ at a constant axial location of $z = 1.5\lambda_0$. It is observed that the computation time for the Sommerfeld integral is lower than the Schelkunoff integral for achieving the same accuracy, as also predicted through the convergence characteristics of the respective kernels in Figure 4c. The computation time with variation in the axial location of the observation point is shown in Figure 7b, with $\rho = 1.5\lambda_0$. The Schelkunoff formulation exhibits a better performance in this case, consistent with the convergence characteristics in Figure 4a.

The number of integration samples N and cylindrical azimuthal harmonics n required for convergence in the main and tail parts of the integral for both formulations is shown in Table 1. The time needed to compute the Sommerfeld and Schelkunoff integrals is also shown for the cases $(\rho - \rho') \gg (z - z')$ and $(z - z') \gg (\rho - \rho')$. It can be observed that the Sommerfeld formulation requires a significantly lesser computation time than the Schelkunoff for $(\rho - \rho') \gg (z - z')$. The difference arises due to the faster converging tail of the Sommerfeld kernel relative to the Schelkunoff tail as can be seen by comparing the number of samples in the Sommerfeld and Schelkunoff tails for this case. This is particularly contributed by the decaying $K_n \left(\rho \sqrt{k_z^2 - k_0^2} \right)$

term in the Sommerfeld tail at a large radial distance. On the other hand, in addition to the presence of the $H_n^{(2)}(k_{\rho 0} \rho)$ term in the Schelkunoff kernel, a relatively low axial separation between the source and field points impedes the exponential decay of the Schelkunoff tail, contributing to its slow convergence.

However, for $(z - z') \gg (\rho - \rho')$, the computation time for the Schelkunoff integral is much lower than the Sommerfeld, that can be principally seen in the large number of samples needed for the convergence of the Sommerfeld tail. This is principally attributed to the exponential decay of the Schelkunoff tail due to the large axial separation between the source and field points. On the other hand, the oscillatory exponential term in the Sommerfeld tail, in addition to the slower radial decay of fields result in its slower convergence, causing about an 85% reduction in the number of samples in the Schelkunoff tail relative to the Sommerfeld.

3.2. Dielectric-Coated Conducting Cylinder

The performance of the Sommerfeld and Schelkunoff formulations for the dielectric-coated conducting cylinder is next investigated. The radius of the inner and outer layer of the cylinder are $a_1 = 0.5\lambda_0$ and $a_2 = 0.55\lambda_0$

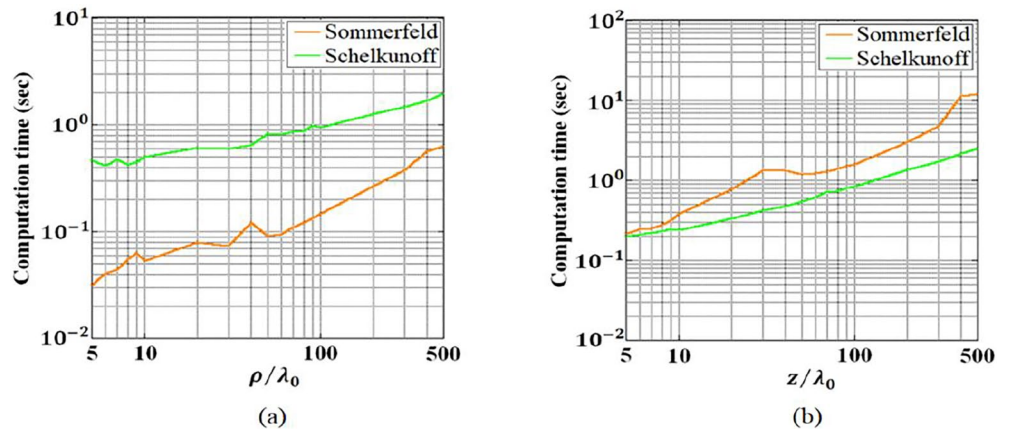


Figure 7. Variation in the computation time for the evaluation of the Sommerfeld and Schelkunoff integrals for the perfectly conducting cylinder with (a) radial location of the observation point at $z = 1.5\lambda_0$ and (b) axial location of the observation point at $\rho = 1.5\lambda_0$. All other parameters same as in Figure 4.

Table 1
Comparison of the Sommerfeld and Schelkunoff Integration for the Conducting Cylinder

Observation point		Sommerfeld formulation					Schelkunoff formulation				
ρ	z	Main part		Tail part		Computation time (sec)	Main part		Tail part		Computation time (sec)
		N	n	N	n		N	n			
$500\lambda_0$	$1.5\lambda_0$	1,575	13	2,569	4	0.6368	1,575	13	4,401	13	1.969
$1.5\lambda_0$	$500\lambda_0$	2,001	14	28,701	11	12.12	2,305	15	4,189	14	2.5321

respectively with a coating permittivity of $\epsilon_{r2} = 2.3$. The location of the dipole is the same as previously. The operating frequency is 5 GHz.

Figure 8a shows the convergence of the Sommerfeld and the Schelkunoff kernels when the axial separation between the observation and source points ($10\lambda_0$) is much larger than their radial separation ($1\lambda_0$). The Schelkunoff kernel is observed to converge much faster than the Sommerfeld in this case. The convergence characteristics of the two formulations are next investigated for equal radial and axial separations between the observation and source points in Figure 8b. The decay rate of both formulations is observed to be the same in this case. The kernel characteristics are then compared for the case when the radial separation is much greater than the axial separation. It is observed that the Sommerfeld formulation converges much faster than the Schelkunoff in this case.

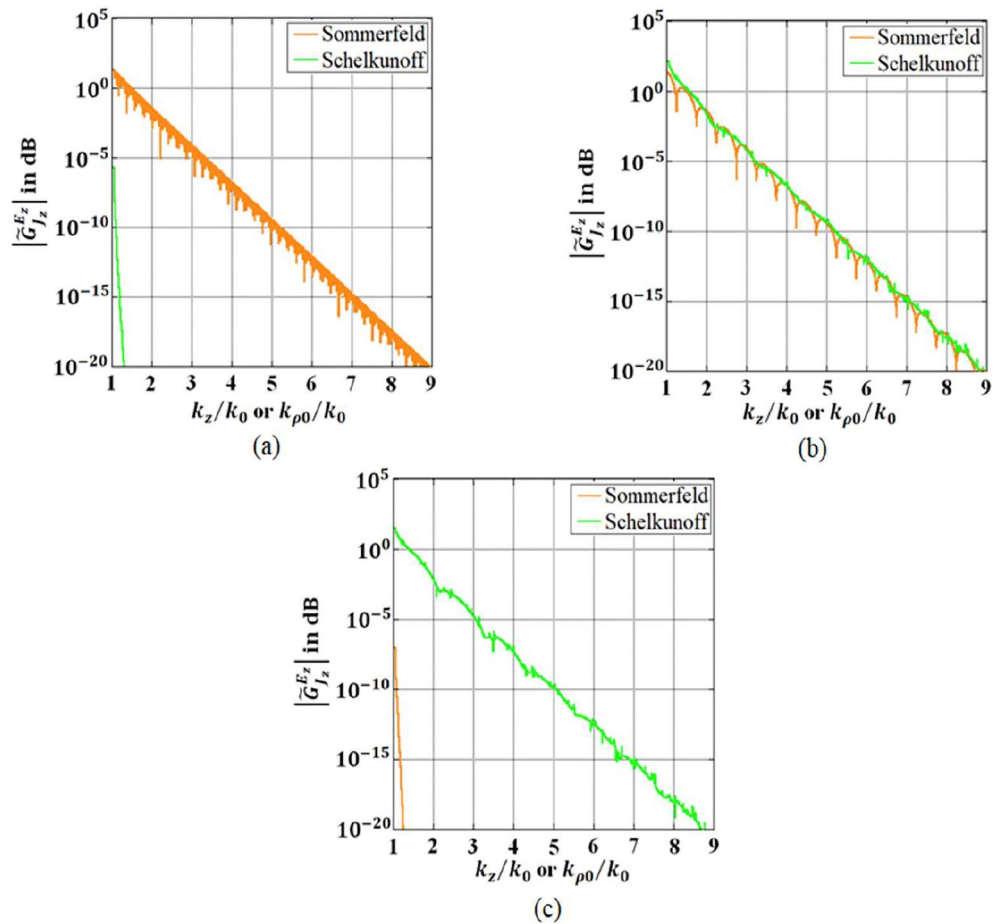


Figure 8. Comparison of the absolute values of the Sommerfeld and the Schelkunoff kernels for the dielectric-coated conducting cylinder with variation in the radial and axial separation between the observation and source points: $a_1 = 0.5\lambda_0, a_2 = 0.55\lambda_0, \rho' = 1\lambda_0,$ and $z' = 0$. (a) $(\rho - \rho') = 1\lambda_0, (z - z') = 10\lambda_0$ (b) $(\rho - \rho') = 1\lambda_0, (z - z') = 1\lambda_0,$ and (c) $(\rho - \rho') = 10\lambda_0, (z - z') = 1\lambda_0$.

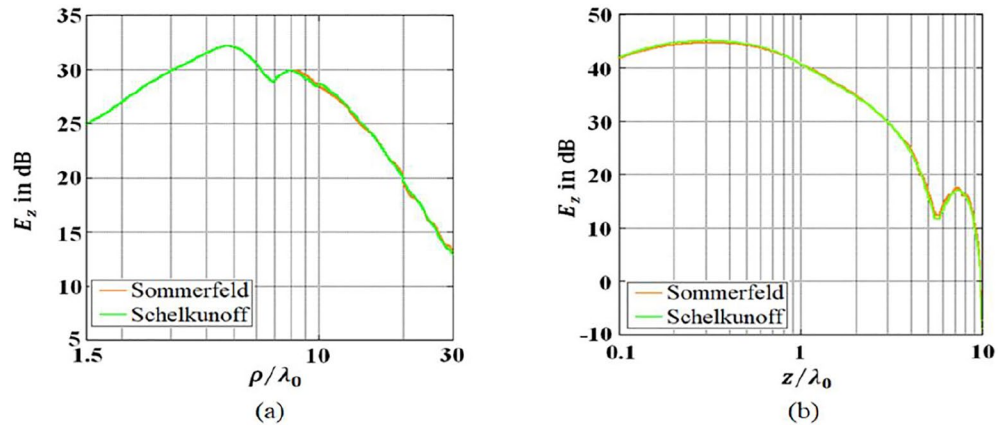


Figure 9. Comparison of the absolute values of the Sommerfeld and the Schelkunoff integrals for the dielectric-coated conducting cylinder at (a) $z = 3\lambda_0$, and (b) $\rho = 3\lambda_0$. All other parameters same as in Figure 8.

The above characteristics reflect similar behavior of the Sommerfeld and Schelkunoff kernels for the conducting cylinder and the coated conducting cylinder configurations. The number of azimuthal modes are taken to be 15 in the above comparisons.

The absolute values of the Sommerfeld and Schelkunoff integrals for the coated conducting cylinder is next investigated. The integrals in this case, obtained through path deformation as described in Section 2.2, are evaluated for the same parameter values as in Figure 8. The absolute value of the spatial domain electric field with the variation in the radial distance is shown in Figure 9a. The axial location of the observation point in this case is at $z = 3\lambda_0$ at 5 GHz while the radial location is varied from $\rho = 1.5\lambda_0$ to $30\lambda_0$. The parameters for path deformation in Equations 33–35 for the Sommerfeld formulation are: $T_1 = 0.5$, $T_2 = 1.5$, $T_3 = 3.5$, and $T_4 = 13$. The Schelkunoff path deformation is performed using $T_1 = 0.5$, $T_2 = 1.5$, $T_3 = 3$, and $T_4 = 13$. It is observed that the Sommerfeld and Schelkunoff integrals match very well for the entire range of variation in ρ . Figure 9b shows the variation of the spatial electric field along the axial direction at $\rho = 3\lambda_0$. The Sommerfeld path deformation parameters for this case are: $T_1 = 0.5$, $T_2 = 1.5$, $T_3 = 2$, and $T_4 = 13$, while for the Schelkunoff case, the following parameters are used: $T_1 = 0.7$, $T_2 = 1.5$, $T_3 = 3$, and $T_4 = 13$. A very good agreement is again observed between the two formulations over the entire range of $0.1\lambda_0 \leq z \leq 10\lambda_0$.

The convergence characteristics of the Sommerfeld and Schelkunoff absolute integral values corresponding to the spatial domain electric field E_z with the order of the cylindrical functions at $z = 3\lambda_0$, $\rho = 3\lambda_0$ is shown in

Figure 10. It can be observed that convergence in both the Sommerfeld and Schelkunoff formulations is obtained after 12 terms.

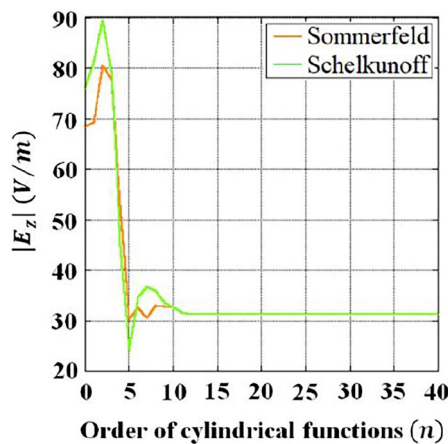


Figure 10. Convergence of the absolute values of the Sommerfeld and the Schelkunoff integrals with order of cylindrical functions for the dielectric-coated conducting cylinder at $z = 3\lambda_0$, $\rho = 3\lambda_0$. All other parameters same as in Figure 8.

The variation in computation time for the two formulations with the radial location of the observation point is shown in Figure 11a at $z = 1.5\lambda_0$. Comparing the results with Figure 7a, a significant enhancement in computation time is observed for the current configuration relative to the conducting cylinder for both the Sommerfeld and Schelkunoff formulations. The computation time for the Sommerfeld formulation that is significantly lower than the Schelkunoff formulation is largely contributed by the integration over Path 2 that is dependent on parameters for path deformation. Figure 11b shows the variation in computation time with the axial location of the observation point at $\rho = 1.5\lambda_0$. For this case as well, the computation time for the better performing Schelkunoff formulation is essentially due to integration over Path 2. However, the difference in the computation times of the Schelkunoff versus the Sommerfeld formulation arises primarily due to their relative performances over Path 3, as is explored further.

Table 2 below demonstrates the characteristics of the Sommerfeld and Schelkunoff integrals with variation in the number of samples (N) and

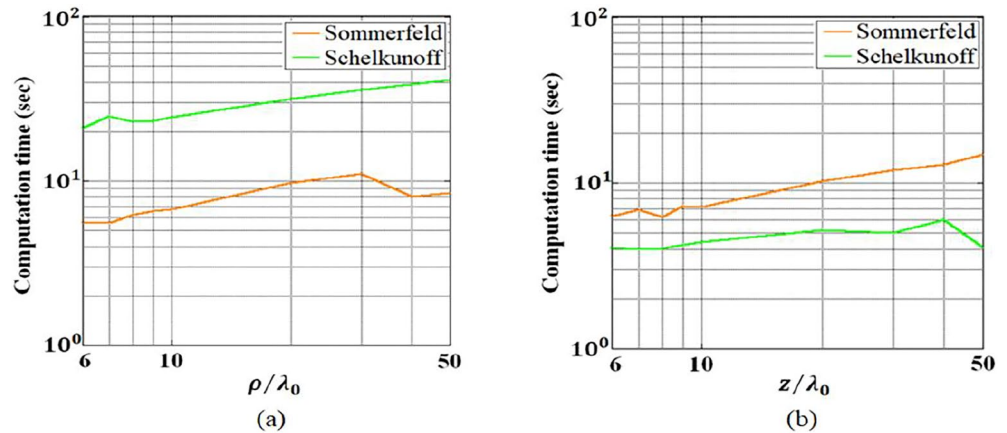


Figure 11. Variation in the computation time for the evaluation of the Sommerfeld and Schelkunoff integrals for the dielectric-coated conducting cylinder with (a) radial location of the observation point at $z = 1.5\lambda_0$ and (b) axial location of the observation point at $\rho = 1.5\lambda_0$. All other parameters same as in Figure 8.

cylindrical harmonics needed for convergence over the deformed integral paths 1, 2 and 3 for the coated conducting cylinder for the cases $(\rho - \rho') \gg (z - z')$ and $(z - z') \gg (\rho - \rho')$. For $(\rho - \rho') \gg (z - z')$, the faster convergence of the Sommerfeld tail over Path 3 relative to the Schelkunoff tail, as evident from the highly reduced number of samples over the Sommerfeld tail relative to the Schelkunoff tail, leads to a reduced computation time for the Sommerfeld formulation. For the case $(z - z') \gg (\rho - \rho')$, the reduced computation time for the Schelkunoff formulation over the Sommerfeld case is contributed by the decaying Schelkunoff tail over Path 3 relative to the Sommerfeld tail. It may be noted that the relative convergence behavior of the two formulations over Path 3 for the current configuration are contributed by similar terms as for the integral tails for the PEC cylinder.

4. Conclusions

The current work presents the rigorous investigation of the Sommerfeld and the Schelkunoff formulations for cylindrical structures. It is observed that the Sommerfeld formulation converges faster than the Schelkunoff formulation for larger radial separation between the source and field points, relative to their axial separation, for both the conducting and the dielectric-coated conducting cylinder. On the other hand, for larger axial separation between the source and field points compared to their radial separation, the Schelkunoff formulation converges more rapidly relative to the Sommerfeld formulation. The above observations are also supported in the comparison of computation times for both formulations. As such, the appropriate formulation can be used depending on the relative radial and axial separation between the source and field points. The work also highlights the distinctive features of cylindrical structures relative to planar structures investigated earlier. Particularly, the presence of higher order Bessel and Hankel functions and azimuthal summation over cylindrical harmonics for cylindrical structures is distinctly different from planar structures that involve the Bessel function of the zeroth order only without any azimuthal summation. As a result, the convergence characteristics for planar structures depend on the Bessel function of zeroth order for the Sommerfeld formulation and the modified Bessel function of zeroth order for the Schelkunoff formulation. On the other hand, convergence behavior for the kernel or the integral value for the Sommerfeld and/or Schelkunoff formulations for cylindrical structures is dominated by complex linear

Table 2
Comparison of the Sommerfeld and Schelkunoff Integration for Dielectric-Coated Conducting Cylinder

Observation point		Sommerfeld formulation							Schelkunoff formulation						
ρ	z	Path 1		Path 2		Path 3		Computation time (sec)	Path 1		Path 2		Path 3		Computation time (sec)
		N	n	N	n	N	n		N	n	N	n			
$50\lambda_0$	$1.5\lambda_0$	87	13	2,543	12	11	5	8.494	129	8	649	13	9,963	27	41.58
$1.5\lambda_0$	$50\lambda_0$	193	12	1,231	11	1,583	24	14.86	83	13	1,483	13	51	3	4.0731

combinations of higher order Bessel/Hankel functions and/or modified Bessel functions. The work presents two cylindrical configurations: a conducting cylinder and a dielectric-coated conducting cylinder that demonstrate two distinct analytical approaches for evaluating the spectral domain integral. Due to the presence of only the branch-point singularity for the case of the conducting cylinder, the relevant spectral integral can be evaluated and the integrable singularity removed by transformation to the β domain. However, due to the presence of poles and branch-point singularities along the real k_z/k_ρ axis for the dielectric-coated conducting cylinder, the Sommerfeld/Schelkunoff integrals are evaluated along a deformed path. An in-depth investigation is carried out on the convergence of the Sommerfeld and Schelkunoff kernels for the cylindrical structures, taking into account the mode coupling between the TE/TM modes in the latter case. In addition, computational aspects for the evaluation of the spectral domain integrals for the cylindrical structures is also examined, including the computation time, number of samples and the number of azimuthal modes to provide a complete perspective towards the performances of the Sommerfeld and Schelkunoff formulations for cylindrical structures.

Data Availability Statement

No external data sets are used for this research.

Acknowledgments

The authors would like to thank the reviewers for their valuable and constructive suggestions.

References

- Bertuch, T., Vipiana, F., & Vecchi, G. (2012). Efficient analysis of printed structures of arbitrary shape on coated cylinders via spatial-domain mixed-potential Green's function. *IEEE Transactions on Antennas and Propagation*, 60(3), 1425–1439. <https://doi.org/10.1109/TAP.2011.2180343>
- Bhattacharya, D., Ghosh, B., & Sarabandi, K. (2017). Evaluation of efficient closed-form Green's function in a cylindrically stratified medium. *IEEE Transactions on Antennas and Propagation*, 65(3), 1505–1510. <https://doi.org/10.1109/TAP.2016.2647706>
- Bhattacharya, D., Ghosh, B., Sinha, M., & Kishk, A. A. (2020). Mode excitation and radiation characteristics of antennas in cylindrically stratified media. *IET Microwaves, Antennas & Propagation*, 14(10), 1027–1037. <https://doi.org/10.1049/iet-map.2020.0044>
- Bhattacharyya, A. K. (2018a). Longitudinal spectral solutions for the Sommerfeld half-space problem: Presenting new perspectives for electromagnetic field solutions in an axially layered structure. *IEEE Antennas and Propagation Magazine*, 60(6), 72–82. <https://doi.org/10.1109/MAP.2018.2870656>
- Bhattacharyya, A. K. (2018b). *New perspectives for the longitudinal spectral solution of Sommerfeld half-space problem*. USNC-URSI Radio Science Meeting. Paper presented at 2018. <https://doi.org/10.1109/APUSNCURSINRSM.2018.8608263>
- Carter, P. S. (1943). Antenna arrays around cylinders. *Proceedings of the IRE*, 31(12), 671–693. <https://doi.org/10.1109/JRPROC.1943.233684>
- Chew, W. C. (1995). *Waves and fields in inhomogeneous media*. IEEE Press.
- Dyab, W., Abdallah, M., Sarkar, T. K., & Salazar-Palma, M. (2013a). On the relation between surface plasmons and Sommerfeld's surface electromagnetic waves. In *Paper presented in 2013 IEEE MTT-S international microwave symposium digest, seattle, WA, USA*. <https://doi.org/10.1109/MWSYM.2013.6697672>
- Dyab, W. M., Sarkar, T. K., & Salazar-Palma, M. (2013b). A physics-based Green's function for analysis of vertical electric dipole radiation over an imperfect ground plane. *IEEE Transactions on Antennas and Propagation*, 61(8), 4148–4157. <https://doi.org/10.1109/TAP.2013.2265377>
- Dyab, W. M. G., Sarkar, T. K., Abdallah, M. N., & Salazar-Palma, M. (2016). Green's function using Schelkunoff integrals for horizontal electric dipoles over an imperfect ground plane. *IEEE Transactions on Antennas and Propagation*, 64(4), 1342–1355. <https://doi.org/10.1109/TAP.2016.2529639>
- Ebihara, S., & Chew, W. C. (2003). Calculation of Sommerfeld integrals for modeling vertical dipole array antenna for borehole radar. *IEICE - Transactions on Electronics*, E86-C(10), 2085–2096.
- Hua, Y., & Sarkar, T. K. (1989). Generalized pencil-of-function method for extracting poles of an EM system from its transient response. *IEEE Transactions on Antennas and Propagation*, 37(2), 229–234. <https://doi.org/10.1109/8.18710>
- Karan, S., & Ertürk, V. B. (2014). Analysis of input impedance and mutual coupling of microstrip antennas on multilayered circular cylinders using closed-form Green's function representations. *IEEE Transactions on Antennas and Propagation*, 62(11), 5485–5496. <https://doi.org/10.1109/TAP.2014.2357413>
- Lucke, W. S. (1951). Electric dipoles in the presence of elliptic and circular cylinders. *Journal of Applied Physics*, 22(1), 14–19. <https://doi.org/10.1063/1.1699813>
- Michalski, K. A., & Mosig, J. R. (2015a). On the surface fields excited by a Hertzian dipole over a layered halfspace: From radio to optical wavelengths. *IEEE Transactions on Antennas and Propagation*, 63(12), 5741–5752. <https://doi.org/10.1109/TAP.2015.2484422>
- Michalski, K. A., & Mosig, J. R. (2015b). The Sommerfeld halfspace problem redux: Alternative field representations, role of Zenneck and surface plasmon waves. *IEEE Transactions on Antennas and Propagation*, 63(12), 5777–5790. <https://doi.org/10.1109/TAP.2015.2489680>
- Moon, H., Teixeira, F. L., & Donderici, B. (2014). Stable pseudoanalytical computation of electromagnetic fields from arbitrarily-oriented dipoles in cylindrically stratified media. *Journal of Computational Physics*, 273, 118–142. <https://doi.org/10.1016/j.jcp.2014.05.006>
- Moon, H., Teixeira, F. L., & Donderici, B. (2015). Computation of potentials from current electrodes in cylindrically stratified media: A stable, rescaled semi-analytical formulation. *Journal of Computational Physics*, 280, 692–709. <https://doi.org/10.1016/j.jcp.2014.10.015>
- Okhmatovski, V. I., & Cangellaris, A. C. (2004). Evaluation of layered media Green's functions via rational function fitting. *IEEE Microwave and Wireless Components Letters*, 14(1), 22–24. <https://doi.org/10.1109/LMWC.2003.821492>
- Papas, C. H. (1949). On the infinitely long cylindrical antenna. *Journal of Applied Physics*, 20(5), 437–440. <https://doi.org/10.1063/1.1698401>
- Sarkar, T. K., Dyab, W., Abdallah, M. N., Salazar-Palma, M., Prasad, M. V. S. N., & Ting, S. W. (2014). Application of the Schelkunoff formulation to the Sommerfeld problem of a vertical electric dipole radiating over an imperfect ground. *IEEE Transactions on Antennas and Propagation*, 62(8), 4162–4170. <https://doi.org/10.1109/TAP.2014.2325591>

- Schelkunoff, S. A. (1936). Modified Sommerfeld's integral and its applications. *Proceedings of the Institute of Radio Engineers*, 24(10), 1388–1398. <https://doi.org/10.1109/JRPROC.1936.227361>
- Tokgoz, C., & Dural, G. (2000). Closed-form Green's functions for cylindrically stratified media. *IEEE Transactions on Microwave Theory and Techniques*, 48(1), 40–49. <https://doi.org/10.1109/22.817470>
- Wait, J. R. (1959). *Electromagnetic radiation from cylindrical structures*. Pergamon.
- Xing, G., Xu, H., & Teixeira, F. L. (2018). Evaluation of ecentered electrode-type resistivity logging in anisotropic geological formations with a matrix method. *IEEE Transactions on Geoscience and Remote Sensing*, 56(7), 3895–3902. <https://doi.org/10.1109/TGRS.2018.2815738>
- Ye, L. F., Chai, S. L., Zhang, H. S., Peng, D., & Xiao, K. (2013). Solving the axial line problem for fast computation of mixed potential Green's functions for cylindrically stratified media. *IEEE Transactions on Microwave Theory and Techniques*, 61(1), 23–37. <https://doi.org/10.1109/TMTT.2012.2228217>